Biochemistry **2006,** *45,* 2577−2583

Solution Structure of an Oncogenic Mutant of Cdc42Hs[†,‡]

Paul D. Adams and Robert E. Oswald*

Department of Molecular Medicine, Cornell University, Ithaca, New York 14853

Received August 24, 2005; Revised Manuscript Received December 23, 2005

ABSTRACT: Cdc42Hs(F28L) is a single-point mutant of Cdc42Hs, a member of the Ras superfamily of GTP-binding proteins, that facilitates cellular transformation brought about by an increased rate of cycling between GTP and GDP [Lin, R., et al. (1997) *Curr. Biol. 7*, 794−797]. Dynamics studies of Cdc42Hs-(F28L)-GDP have shown increased flexibility for several residues at the nucleotide-binding site [Adams, P. D., et al. (2004) *Biochemistry 43*, 9968−9977]. The solution structure of Cdc42Hs-GDP (wild type) has previously been determined by NMR spectroscopy [Feltham, J. L., et al. (1997) *Biochemistry 36*, 8755−8766]. Here, we describe the solution structure of Cdc42Hs(F28L)-GDP, which provides insight into the structural basis for the change in affinity for GDP. Heteronuclear NMR experiments were performed to assign resonances in the protein, and distance, hydrogen bonding, residual dipolar coupling, and dihedral angle constraints were used to calculate a set of low-energy structures using distance geometry and simulated annealing refinement protocols. The overall structure of Cdc42Hs(F28L)-GDP is very similar to that of wild-type Cdc42Hs, consisting of a centrally located six-stranded β-sheet structure surrounding the C-terminal α-helix [Feltham, J. L., et al. (1997) *Biochemistry 36*, 8755−8766]. In addition, the same three regions in wild-type Cdc42Hs that show structural disorder (Switch I, Switch II, and the Insert region) are disordered in F28L as well. Although the structure of Cdc42Hs(F28L)-GDP is very similar to that of the wild type, interactions with the nucleotide and hydrogen bonding within the nucleotide binding site are altered, and the region surrounding L28 is substantially more disordered.

The Ras superfamily of GTP-binding proteins is involved in a variety of cellular processes such as cell growth, protein trafficking, cytoskeletal organization, and secretion. The proteins are controlled by cycling between the biologically active GTP[1] form and the inactive GDP-bound form (*1*, *2*). GTP is hydrolyzed to GDP by the intrinsic GTPase activity of the protein; however, the cycle of binding, hydrolysis, and rebinding of the nucleotide is controlled by a number of regulatory and effector proteins (*3*−*5*). The Ras proteins, especially the Rho subfamily, have been extensively investigated because of their potential roles in cell transformation. Oncogenic Ras proteins transform cells due to either a defect in GTPase activity, which leads to a terminally active state, or an increased rate of GTP−GDP cycling. In either case, the activity of downstream kinases is increased. Point mutations in Ras that inhibit the GTPase activity (e.g., G12V and Q61L) have been implicated in several types of cancer (*6*−*8*). In addition, the F28L mutation in Cdc42Hs (a member of the Rho subfamily) results in cell transformation due to the increased rate of cycling between the active and inactive forms of the protein. The mutation-induced cell transformation by Cdc42Hs(F28L) is similar to the cell transformation induced by the Dbl oncoprotein, which also catalyzes fast nucleotide exchange in Cdc42Hs (*3*).

Structural studies of wild-type Cdc42Hs-GDP (*9*) as well as H-Ras-GDP (*10*, *11*) and Rac-GDP, another member of the Ras superfamily (*12*), have elucidated several well-conserved regions in these proteins. However, unique structural aspects of each of these proteins provide specificity for various effector and/or regulatory proteins. In all three cases, the bound nucleotide interacts with the same regions: P loop or loop 1 (residues 10−15), residues 116−119 (residues 115−118 in Cdc42Hs), residues 145−147 (residues 158−160 in Cdc42Hs), and F^{28}. F^{28} serves as the principal stabilizer of the nucleotide via a strong interaction with the aromatic ring of the bound nucleotide (*10*, *13*, *14*). When F^{28} is mutated to leucine, this interaction is lost. ^{31}P NMR studies have shown chemical shift differences in the bound phosphates in H-Ras p21(F28L) relative to wild-type H-Ras (*14*). In addition, Cdc42Hs(F28L)-GDP (*15*) as well as Ras-(F28L) (*14*, *16*) shows a drastic increase in the GDP dissociation rate in the F28L mutant relative to that of the wild type, suggesting that F^{28} is an important contributor to the stability of GDP binding. NMR dynamics studies of Cdc42Hs(F28L)-GDP (*17*) have shown several differences

---

[†] This material is based upon work supported by the National Science Foundation under a grant awarded to P.D.A. in 2002 and by a grant from the National Institutes of Health (R01 GM56223) to R.E.O.

[‡] The coordinates of Cdc42Hs(F28L)-GDP have been deposited with the Protein Data Bank as entry 2ASE.

* To whom correspondence should be addressed: Department of Molecular Medicine, College of Veterinary Medicine, Cornell University, Ithaca, NY 14853. Phone: (607) 253-3877. Fax: (607) 253-3659. E-mail: reo1@cornell.edu.

[1] Abbreviations: F28L, mutation of phenylalanine 28 in Cdc42Hs to leucine; GDP, guanosine 5′-diphosphate; GTP, guanosine 5′-triphosphate; GAP, GTPase activating protein; GEF, guanidine nucleotide exchange factor; GDI, guanidine nucleotide dissociation inhibitor; HSQC, heteronuclear single-quantum correlation; IPTG, isopropyl β-D-thiogalactopyranoside; NMR, nuclear magnetic resonance; NOE, nuclear Overhauser effect; RDC, residual dipolar coupling; P loop or loop 1, residues 10−15 of Cdc42Hs; Switch I, residues 31−40 of Cdc42Hs; Switch II, residues 57−74 of Cdc42Hs; Insert region, residues 121−134 of Cdc42Hs.

10.1021/bi051686g CCC: $33.50

in flexibility at the nucleotide-binding site of Cdc42Hs-(F28L)-GDP relative to that of the wild type (*18*), while the dynamics of the remainder of the protein are not significantly altered by the mutation.

In this paper, we present the solution structure of the single-point mutant Cdc42Hs(F28L)-GDP. Analysis of the solution structure of Cdc42Hs(F28L)-GDP in comparison to wild-type Cdc42Hs (*9*) shows that, overall, the core of Cdc42Hs(F28L)-GDP is very similar to the wild-type structure. In the mutant protein, however, some of the regions comprising the nucleotide-binding site exhibit differences that may explain the increase in the GDP dissociation rate. Further, the regions that show the most pronounced differences in stabilizing interactions with the nucleotide correlate with the regions of the protein with the greatest changes in dynamics relative to that of the wild type (*17*).

EXPERIMENTAL PROCEDURES

Protein Expression and Purification. A Cdc42Hs construct with a C-terminal truncation (*19*) was used to prepare the F28L mutation. The construct was cloned into a pET-15b vector and subsequently overexpressed in *Escherichia coli*. Cultures (5 mL) were initially grown to saturation and used to seed 1 or 2 L cultures grown in LB broth for natural-abundance samples, and in minimal media containing $^{15}NH_4Cl$ as the sole nitrogen source for ^{15}N-labeled samples. Expression and purification proceeded as outlined previously (*17*). For two-dimensional (2D) NMR experiments using ^{15}N-labeled GDP, unlabeled wild-type Cdc42Hs and Cdc42Hs-(F28L)-GDP samples were prepared as described above except that natural-abundance NH_4Cl was used, and 0.1 mM [^{15}N]GDP was incorporated in all buffers throughout purification. Expression levels using [^{13}C]glucose were too low to produce ^{15}N- and ^{13}C-labeled protein for triple-resonance and $^1H-^{13}C$ NOESY-HSQC experiments.

NMR Spectroscopy. All protein samples were prepared in an NMR sample buffer solution containing 25 mM NaCl, 10 mM NaH_2PO_4, 5 mM $MgCl_2$, and 1 mM NaN_3 with 8% D_2O at pH 5.5 at Cdc42Hs(F28L)-GDP concentrations of 0.2−0.5 mM in volumes of ∼250 μL. NMR spectra were recorded using Varian Inova 600 and 500 MHz spectrometers. The 600 MHz spectrometer was equipped with a triple-resonance pulsed-field gradient probe and the 500 MHz spectrometer with a triple-resonance cryogenic probe. All NMR spectra were acquired at 25 °C in States−TPPI mode for quadrature detection (*20*). Carrier frequencies for ^1H and ^{15}N were 4.77 and 115.9 ppm, respectively. 2D $^1H-^{15}N$ HSQC spectra were acquired on ^{15}N-labeled Cdc42Hs-(F28L)-GDP. A 2D NOESY experiment was performed using a natural-abundance sample (in 100% D_2O) to detect side chain−side chain NOE peaks for some residues with relatively isolated methyl resonances. Hydrogen−deuterium exchange was assessed by lyophilizing the sample and resuspending it in 100% D_2O. A series of $^1H-^{15}N$ HSQC experiments were performed at 0, 5, 15, 25, and 60 min, and the decrease in the volume and eventual disappearance of $^1H-^{15}N$ cross-peaks were used to determine the extent of exchange of deuterons for protons. Three-dimensional (3D) $^1H-^{15}N$ TOCSY-HSQC experiments were acquired with mixing times of 50 and 70 ms. 3D $^1H-^{15}N$ NOESY-HSQC spectra were acquired using a mixing time of 125 ms.

NMR spectra were processed using NMRPipe, version 1.6 (*21*). The spectra were zero-filled and then apodized using a Gaussian window function prior to Fourier transformation. After Fourier transformation, a baseline correction was applied. Spectra were visualized and analyzed using Xeasy (version 1.3.6) (*22*). Peaks were integrated using Peakint (N. Schaefer, Diploma Thesis, ETH, Zurich, Switzerland). The backbone proton and nitrogen assignments for Cdc42Hs-(F28L)-GDP were reported previously (*17*). We were able to assign a majority of the Hα, Hβ, Hδ, and Hγ protons by analysis of the $^1H-^{15}N$ TOCSY-HSQC and $^1H-^{15}N$ NOESY-HSQC spectra of Cdc42Hs(F28L)-GDP overlaid with the corresponding spectra of the wild type. More than 90% of the side chain protons had similar chemical shifts. Residues in two stretches, $T^{35}-N^{39}$ (Switch I region) and G^{60} and $R^{65}-R^{68}$ (Switch II region) in Cdc42Hs(F28L)-GDP, were unassigned due to line broadening resulting from conformational dynamics, similar to that observed for wild-type Cdc42Hs (*9*).

For residual dipolar coupling (RDC) measurements, a [^{15}N]-Cdc42(F28L)-GDP sample was partially aligned in the magnetic field (Varian Inova 500) with a nonionic liquid crystalline medium made up of 4% C12E6 [*n*-dodecyl hexa-(ethylene glycol)] and *n*-hexanol (*23*). Alignment was verified using the quadrupolar splitting of the ^2H spectrum. RDCs were determined from partially aligned and unaligned samples using TROSY experiments with the phase cycling adjusted to observe the two nitrogen components individually.

Structure Calculation. $^1H-^{15}N$ NOESY-HSQC experiments were used to derive distance constraints. A majority of the resonances for Cdc42Hs(F28L)-GDP were similar to the corresponding resonances of the wild type, making the NOE assignment relatively straightforward. The volumes of several well-dispersed and isolated sequential $d_{\alpha N}$ and $d_{\alpha N}(i,j)$ NOE peaks (resulting from correlation within and between parallel β-strands, respectively) were calibrated to the distances expected for ideal β-sheets (2.2 and 3 Å, respectively). NOESY constraints were classified according to their relative strength in the NOESY spectrum (<2.4, <3.4, <4.0, and <5.5 Å). Also, 55 hydrogen bond constraints were input into the structure calculations based on H−D exchange studies by NMR, the chemical shift index (indicating α-helix or β-sheet) (*24*, *25*), and expected NOE patterns indicative of hydrogen bonding. For each hydrogen bond, the distance between the amide proton and the carbonyl oxygen for the residue was constrained to be 1.8−2.3 Å, and the amide nitrogen−carbonyl oxygen distance was constrained to be between 2.5 and 3.3 Å (*9*). Dihedral constraints were included for residues in α-helices and β-sheets (for α-helix, $\phi = -80 \pm 50°$ and $\psi = -20 \pm 50°$; for β-sheet, $\phi = -105 \pm 65°$ and $\psi = 145 \pm 45°$). Sixty-eight RDCs from well-resolved resonances were used as additional constraints. All constraints were input into Xplor-NIH (*26*) to calculate an ensemble of structures for the protein. The 15 "best" structures from 600 calculated structures were selected on the basis of their overall low energies and minimal constraint violations. The experimental statistics from the structure calculations are given in Table 1. The structures were visualized using Swiss PDBviewer (version 3.7) (*27*) and MacPyMol (*28*) and analyzed using AQUA (*29*), PROCHECK-NMR (*29*), and the NMR en-

Table 1: Statistics and Restraint Data for the Structure Calculation of Cdc42Hs(F28L)

	ensemble of 15 structures	most representative structure
rmsd from experimental constraints		
NOE distances (Å)	0.08 ± 0.002	0.07
dihedral angles (deg)	0.99 ± 0.15	0.83
rmsd from secondary structure		
bonds (Å)	0.003 ± 0.0006	0.003
angles (deg)	0.56 ± 0.01	0.57
impropers (deg)	0.48 ± 0.02	0.46
Restraint Data		
long-range NOEs ($\|i - j\| > 4$)		461
medium-range NOEs ($4 > \|i - j\| > 1$)		401
total NOEs		862
intramolecular		361
sequential		255
medium-range		111
long-range		134
hydrogen bond		71 × 2
Ψ		92
Φ		90
NH backbone RDC restraints		68

semble program OLDERADO (*30*). For Cdc42Hs(F28L)-GDP, very few intermolecular NOEs were observed between GDP and the protein (except for the N1 proton of the guanine ring), making it impossible to properly constrain GDP in the protein for the structure calculations. There was also a lack of NOE data for the wild type as only two NOEs were observed between the protein and the bound nucleotide (*9*), one of which involved the side chain proton of F^{28} not expected in the mutant protein. The position of the GDP was determined starting with superimposition of the Cdc42Hs-GDP crystal structure onto the core C_α atoms of each of the final 15 Cdc42Hs(F28L) structures, similar to that done for GDP in wild-type Cdc42Hs (*9*). The nucleotide was then copied into the Cdc42Hs(F28L) structure from its position in the crystal structure of wild-type Cdc42Hs. The Cdc42Hs-(F28L)-GDP structures were energy minimized to find the most favorable positions of the nucleotide in the protein. After minimization, NOEs that were observed between the N1 proton of the nucleotide ring and various residues of the protein were used to back calculate distances between the residues and the nucleotide ring. These distances between the N1 proton of the ring and other protons were checked in the structures and found to be compatible with observed NOEs.

RESULTS AND DISCUSSION

Overall Structure of Cdc42Hs(F28L)-GDP. We have determined the 3D solution structure of Cdc42Hs(F28L)-GDP to characterize (1) differences in the nucleotide-binding region in Cdc42Hs(F28L)-GDP that may be consistent with the dynamics results, (2) conformational changes outside of the nucleotide-binding site that may be involved in effector binding, and (3) changes resulting from the lost interaction between the nucleotide base and the phenyl ring of F^{28}. A set of 15 superimposed structures of Cdc42Hs(F28L)-GDP is shown in Figure 1A. The core of the protein [atoms in the protein as defined by OLDERADO (*30*) whose positions are well-defined and largely invariant across the ensemble of structures] gave an rmsd from the average structure of 0.87 ± 0.03 Å for backbone non-hydrogen atoms (Figure 1B). The core atoms of the Cdc42Hs(F28L)-GDP structures are residues 3−9, 16−24, 27, 29, 41−47, 49−56, 75−85, 90−103, 108−116, 136, 139−155, and 161−177, very similar to the core atoms of the final structures of wild-type Cdc42Hs (*9*). Distance, hydrogen bonding, dihedral, and residual dipolar coupling restraints were used to calculate the structure of Cdc42Hs(F28L)-GDP. The secondary structure of Cdc42Hs(F28L)-GDP was determined on the basis of analysis of H−D exchange data, Ramachandran plots of the ensemble of structures, characteristic NOE patterns for secondary structure motifs, and the chemical shift index (*24*, *25*). There were no secondary structural differences in F28L relative to the wild type; the mutant protein also consists of a centrally located six-stranded β-sheet structure surrounding the C-terminal helix of the protein (Figure 1C). Other structural features found in both the wild type and Cdc42Hs-(F28L)-GDP included helices $\alpha3$ and $\alpha4$ flanking the convex surface of the β-sheet, helix $\alpha1$ lying perpendicular to the β-sheet on the concave side of the sheets, and a short αI (Insert) helix lying adjacent to a loop connecting $\beta4$ and $\alpha3$ in the protein (Figure 3C). Also consistent with the wild type are the three regions in Cdc42Hs(F28L)-GDP that show the most structural disorder: Switch I, Switch II, and the Insert region. The disorder in Switches I and II is key to the docking of effector proteins with Cdc42Hs (*18*) and other Ras proteins (*31*).

Structure of the Nucleotide-Binding Site in Cdc42Hs-(F28L)-GDP. Dynamics studies have shown increased flexibility in residues of the nucleotide-binding site in Cdc42Hs-(F28L)-GDP that could affect the signaling processes of Cdc42Hs (*17*). The nucleotide-binding site of Cdc42Hs consists of several regions that have been described from the crystal structures of Cdc42Hs (PDB entry 1ANO) and H-Ras (*31*). The side chain hydroxyl group of T^{35}, the main chain NH group of G^{60}, and P loop residues 10−15 (GXG-XXG motif) interact with the phosphates of the nucleotide. Residues 115−118 interact with one side of the guanine ring of the nucleotide, while residues 28 and 158−160 interact with the opposite side of the guanine ring. Resonances for T^{35} and G^{60} could not be assigned, presumably because they are located in the flexible Switch regions of the protein. Figure 2 shows the remaining nucleotide-binding site residues of 15 low-energy structures of Cdc42Hs(F28L)-GDP with the core atoms of the protein superimposed. Figure 3 shows the sequence-dependent number of interresidue NOEs, the rmsds of the C_α atoms, and the order parameters (*17*) of Cdc42Hs(F28L)-GDP compared to that of the wild type. Because of the differences in the number of NOEs used in the wild type and F28L and the use of RDC restraints for F28L, the rmsd values are not directly comparable. For that reason, specific regions of the each protein are compared to the relatively well-defined core of the protein. The rmsd value for nucleotide-binding site residues (10−15, 28, 115−118, and 158−160) is increased 52% relative to the protein core, in comparison to a 46% increase for the corresponding residues in the wild type (Table 2), with the most striking increase in rmsd surrounding residue 28. Some flexibility in the nucleotide-binding site is expected to facilitate proper cycling of GTP to GDP in Cdc42Hs, but the increased rmsd, particularly in the region of L^{28}, may play a role in the increased rate of nucleotide dissociation.

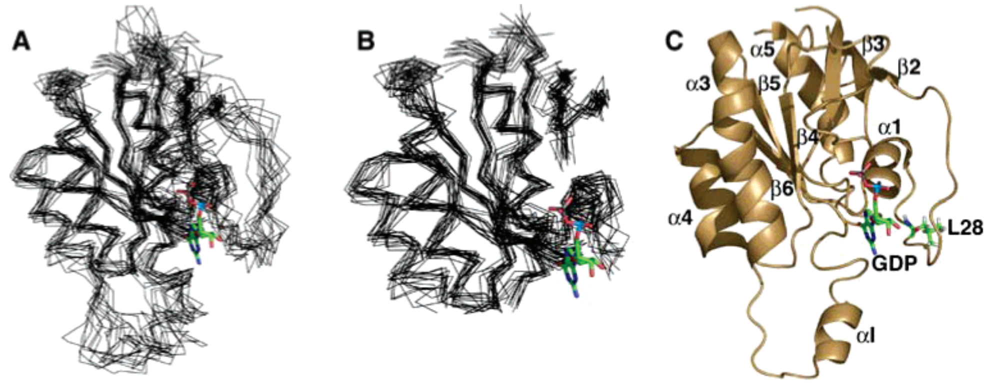

FIGURE 1: Structure of Cdc42Hs(F28L)-GDP. The 15 lowest-energy structures were superimposed (using the core residues indicated in the text) on the average structure generated by Xplor-NIH using MacPyMol (*28*). The nucleotide was superimposed on the structures from the coordinates of the crystal structure of wild-type Cdc42Hs-GDP (PDB entry 1AN0): (A) overlay of the entire structure, (B) overlay with the Switch I and II and the Insert helix removed, and (C) a diagram of the most representative structure [defined by OLDERADO (*30*)] showing the secondary structure.

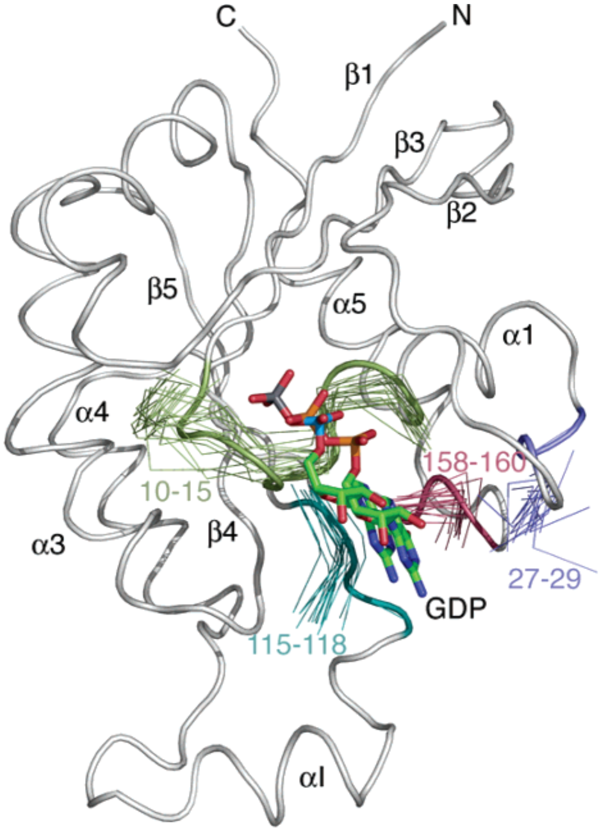

FIGURE 2: Ribbon diagram of the crystal structure of wild-type Cdc42Hs (PDB entry 1AN0) with segments of the 15 lowest-energy structures of Cdc42Hs(F28L)-GDP representing the binding pocket. All structures were superimposed on the average structure computed from the 15 structures shown in Figure 1A.

The principal stabilizing factor for the nucleotide in its binding site is F^{28}. Studies have shown that mutation of this amino acid to leucine increases the GDP dissociation rate significantly in Ras (*14*, *16*) and Cdc42Hs (*15*). An examination of this region in the crystal structure of wild-type Ras (*10*, *14*) and Cdc42Hs (PDB entry 1AN0) shows that the phenyl ring of F^{28} is perpendicular to the guanine ring of the bound nucleotide and serves to stabilize the nucleotide in the binding pocket, an interaction not possible in Cdc42Hs-(F28L)-GDP. The rmsd for the backbone atoms of L^{28} is 84% greater than that of the core of the mutant protein, whereas the difference in rmsd for F^{28} relative to its core in the wild type is negligible (11%, Table 2). Dynamics studies also showed that the backbone of L^{28} in Cdc42Hs(F28L)-GDP exhibits an increased amplitude of local motion relative to the rest of the protein (*17*), suggestive of conformational disorder for the L^{28} backbone not seen for F^{28} in the wild type. Additionally, the crystal structure of wild-type Cdc42Hs shows that a hydrophobic interaction between the side chain of F^{28} and L^{160} (another nucleotide-binding site residue) acts to help orient the phenyl side chain (PDB entry 1ANO). As judged from the lack of NOE cross-peaks between the side chain of L^{28} and L^{160}, this interaction is lost with the F28L mutation, contributing to the diminished stability of the nucleotide in Cdc42Hs(F28L)-GDP.

The P loop region (residues 10−15) interacts with the phosphate groups of the bound nucleotide. Both wild-type Cdc42Hs-GDP and Cdc42Hs(F28L)-GDP exhibit some conformational disorder in this region (Table 2). However, dynamics studies have suggested that the P loop residues of Cdc42Hs(F28L)-GDP display more chemical exchange than the corresponding residues in the wild type. Also, the chemical environment of the P loop residues is different in F28L and the wild type, as suggested by significant chemical shift differences for most of these residues (*17*). Analysis of the wild-type NOESY spectra shows that there are several backbone NH NOEs between residues of the P loop and helix α3 (D^{10} NH−N^{92} Hδ, D^{11} NH−W^{97} Hϵ, and G^{12} NH−W^{97} HNϵ) and residues 116−118. These interactions help stabilize the phosphate region of the bound nucleotide (*11*). Only the D^{11} NH−W^{97} Hϵ NOE is seen in the NOESY spectrum of F28L. In addition, all six residues of the P loop undergo H−D exchange in F28L, while only residues 12 and 14 exhibit H−D exchange in the wild type. In addition, hydrogen bonding networks between the backbone NH groups of residues 16−18 and the α- and β-phosphate groups of the bound nucleotide evident in wild-type Cdc42Hs, which help stabilize the phosphates of the nucleotide (PDB entry 1AN0), are much weaker in Cdc42Hs(F28L)-GDP (*17*). NOEs observed in wild-type Cdc42Hs between the NH groups of T^{17} and C^{18} and the Hϵ protons of Q^{116}, a residue in another region directly interacting with the nucleotide, are weak or nonexistent in F28L. Although not obvious from the average solution structure, the apparently weaker hydrogen bonds and flexibility on the microsecond to millisecond time scale (*17*) may contribute to a greater degree of

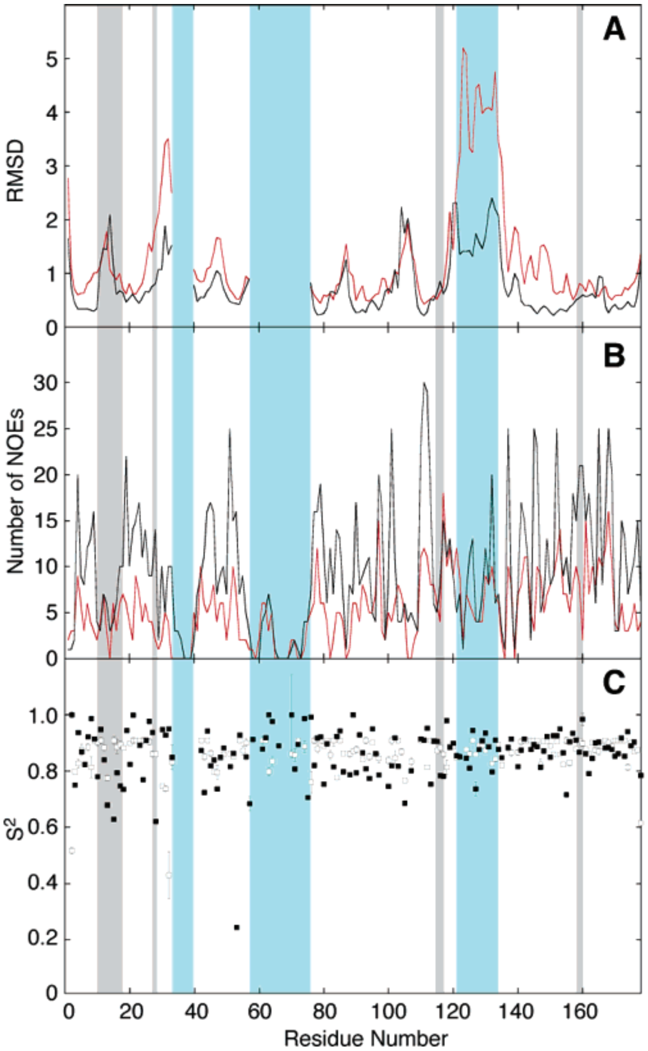

FIGURE 3: Distribution of (A) rmsd values of the C_α atom, (B) the number of interresidue NOEs per residue, and (C) the order parameter (*17*) for Cdc42Hs-GDP and Cdc42Hs(F28L)-GDP. The wild-type data in panels A and B were taken from ref *9* and are colored black [the Cdc42(F28L) data are colored red]. The data in panel C were from ref *17*, and the wild-type data are shown with empty squares and the Cdc42Hs(F28L) data with filled squares. The gray boxes indicate the positions of the nucleotide-binding pocket, and the blue boxes indicate the positions of Switch I, Switch II, and the Insert region. The Switch I and II regions are poorly defined, and the rmsd values have been removed. The difference between the insert region of the wild type and F28L arises largely due to the unavailability of the ^{13}C-separated NOESY experiment for F28L (see Experimental Procedures). Although still poorly defined relative to the core of the protein, the structure is somewhat more constrained in the wild type due to several long-range side chain−side chain NOEs.

Table 2: Percent Increase in Backbone rmsd (%ΔR)[a] for Regions in the Nucleotide-Binding Site Relative to the Average rmsd Value of the Protein Core[b]

	Cdc42Hs-GDP	Cdc42Hs(F28L)-GDP
%ΔR for all backbone atoms in the nucleotide-binding site (10−15, 115−118, 158−160, 28)	46.0	52.0
%ΔR(10−15)	56.0	62.0
%ΔR(115−118)	47.0	65.0
%ΔR(158−160)	0.0	31.0
%ΔR(28)	11.0	84.0

[a] Where %$\Delta R = |\text{rmsd}_{\text{region}}/\text{rmsd}_{\text{core}} - 1| \times 100$. [b] Cdc42Hs-GDP $\text{rmsd}_{\text{core}} = 0.59$ (*9*).

Table 3: NH NOEs for Cdc42Hs (wild type) and Cdc42Hs(F28L) for Residues Comprising the Nucleotide-Binding Site

Cdc42Hs (wild type)	Cdc42Hs(F28L)
11 HN−92 Hδ	11 HN−97 HNϵ
11 HN−97 HNϵ	12 HN−61 Hα
12 HN−97 HNϵ	
15 HN−85 Hγ	
17 HN−116 Hϵ	
18 HN−28 Hϵ	
18 HN−116 Hϵ	
28 HN−160 Hδ	28 HN−160 Hδ
116 HN−158 Hα	116 HN−158 Hα
116 HN−159 Hβ	
	117 HN−161 Hγ
117 HN−158 Hα	117 HN−161 HN
	117 HN−84 HN
118 HN−158 Hα	
118 HN−160 Hδ	118 HN−161 Hγ
158 HN−117 Hγ	
158 HN−117 Hδ	
157 HN−117 Hγ	
158 HN−117 Hγ	158 HN−117 HN
158 HN−117 Hδ	158 HN−117 Hα
159 HN−117 Hγ	159 HN−27 HN
	159 HN−117 HN
160 HN−28 Hδ	160 HN−28 HN

conformational freedom for the nucleotide and an increased rate of dissociation.

The guanine base of the nucleotide is also stabilized via interactions with residues 115−118 on the side of the nucleotide ring opposite F^{28} and with residues 158−160 perpendicular to the nucleotide ring on the same side of the nucleotide as F^{28} (PDB entry 1ANO). Studies of H-Ras have shown that the principal function of residues 116−119 (residues 115−118 in Cdc42Hs) is to provide a link between the other regions of the protein involved in nucleotide binding: the P loop residues and residues 145−147 (158−160 in Cdc42Hs) (*31*). The chemical shifts for these residues differ little between the wild type and F28L (*17*), indicating that the chemical environment is similar. Also, the dynamics parameters for these residues are similar in both the wild type and F28L (*17*). Likewise, little change is seen in the solution structures of the two forms of Cdc42Hs (Figure 2 and Table 2). Despite similarities between the wild type and F28L, several NOEs are observed in wild-type Cdc42Hs between the backbone NH groups of residues 115−118 and other regions that are absent in the F28L spectra (Table 3). The structure of wild-type Cdc42Hs shows that the NH group of Q^{116} has a hydrogen bond with the carbonyl of C^{157} and D^{118} is hydrogen-bonded to the hydroxyl side chain of S^{158} helping to form a tight binding pocket for the nucleotide. In F28L, these two hydrogen bonds are weak or nonexistent as H−D exchange is seen for the backbone NH group of Q^{116} and D^{118}.

The structure of F28L in the region of residues 158−160 shows a small increase in the rmsd (%$\Delta R = 31$), while the corresponding region in the wild type shows no change in rmsd relative to its core (%$\Delta R \approx 0$). The chemical shift difference for these residues between the wild type and F28L is also significant, indicating that these residues lie in a different chemical environment in Cdc42Hs(F28L)-GDP (*17*). In addition, several more NOEs are observed between

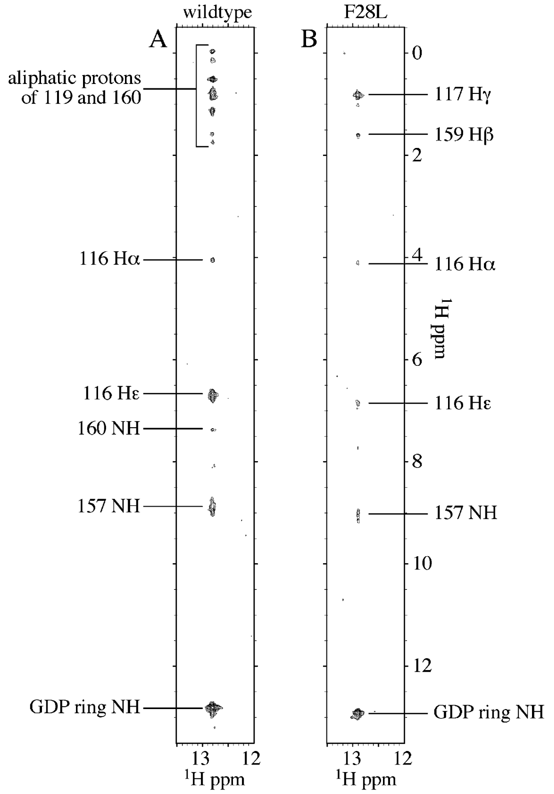

FIGURE 4: ^{1}H−^{15}N NOESY-HSQC spectrum of [^{15}N]GDP bound to wild-type (A) and F28L (B) Cdc42Hs-GDP. The experiment was carried out in two dimensions, with an INEPT sequence filtering only protons bound to nitrogen prior to detection.

the backbone NH group of these residues and other residues in the nucleotide-binding site for the wild-type protein than for F28L (Table 3). In the crystal structure of Cdc42Hs (PDB entry 1ANO), the backbone NH group of S^{158} is hydrogen bonded to the carbonyl of K^{163} while the backbone NH groups of A^{159} and L^{160} are hydrogen bonded to the carbonyl oxygen of the guanine ring. All three of these hydrogen bonding interactions are weak or missing in F28L as determined from H−D exchange experiments.

The Nucleotide. Compelling evidence of conformational differences at the nucleotide-binding site in Cdc42Hs(F28L)-GDP relative to the wild type come from the 2D NMR spectrum with ^{15}N-labeled GDP complexed to both proteins (Figure 4). The N1 proton of the guanine ring in the wild-type complex has a chemical shift of 12.81 ppm versus a shift of 12.92 ppm in the Cdc42Hs(F28L)-GDP complex. This finding is indicative of a more polar environment for the proton in the F28L complex due to either more solvent exposure or a stronger interaction with a more electron-rich group (*32*, *33*). NMR analysis of [^{15}N]GDP-bound Cdc42Hs and Cdc42Hs(F28L)-GDP shows that the nucleotide makes more contacts with residues of the nucleotide-binding site in the wild type than in Cdc42Hs(F28L)-GDP. The ^{1}H−^{15}N NOESY-HSQC spectra of Cdc42Hs-[^{15}N]GDP and Cdc42Hs-(F28L)-GDP-[^{15}N]GDP show NOE cross-peaks involving the nucleotide N1 proton and residues 116 and 157 in both proteins. However, several cross-peaks involving the nucleotide N1H group and residues 119 and 160 in the spectrum of wild-type [^{15}N]GDP are not observed in the corresponding spectrum of Cdc42Hs(F28L)-[^{15}N]GDP. Likewise, the ^{1}H−^{15}N NOESY-HSQC spectrum of Cdc42Hs(F28L)-[^{15}N]GDP shows two NOE cross-peaks involving Hγ of residue 117 and Hβ of residue 159 that were not evident for the wild type, suggestive of a conformational change involving the nucleotide that brings the N1H group of the nucleotide ring into the proximity of both the A^{159} Hβ and I^{117} Hγ protons in Cdc42Hs(F28L)-GDP. These studies reveal several different contacts between the nucleotide and residues of the wild-type protein versus those in F28L due perhaps to a number of lost interactions in the nucleotide-binding site for Cdc42Hs(F28L)-GDP.

Summary. We have shown previously that this single-point mutation leads to increased flexibility on multiple time scales for most of the residues comprising the nucleotide-binding site as well as the nucleotide itself (*17*). We show here that although the structural changes are subtle, the interactions within the nucleotide-binding pocket, both within the protein and between the protein and nucleotide, likely contribute to the decrease in affinity for the nucleotide. NMR studies on H-Ras p21(F28L) indicated that the mutation distorted the binding site around the α- and β-phosphate groups, but the area surrounding the γ-phosphate group was undisturbed (*34*). While this study does not address the γ-phosphate of the nucleotide because only the GDP form has been studied here, our results do show that the conformational differences in this mutant are not confined to the site of the mutation and that the entire nucleotide-binding site of Cdc42Hs(F28L)-GDP is disturbed.

Most oncogenic Ras proteins are locked in a perpetually active state (GTP-like state) and transduce signals that are directly involved in proliferation, transformation, or tumorigenesis (*35*). Mutations that alter the intrinsic ability of the protein to hydrolyze GTP to GDP and affect proper exchange may facilitate oncogenesis (*1*, *11*, *36*). Therefore, these proteins and the signal transduction pathways that help to regulate them are important targets for anticancer therapy. As mentioned previously, Cdc42Hs(F28L)-GDP mimics the fast nucleotide exchange and transformation capability caused by an interaction of wild-type Cdc42Hs with the Dbl oncoprotein (*37*). These studies describing the structural correlates of the F28L mutation in Cdc42Hs have provided important molecular information about the protein's function and will be extended to other mutations that affect normal functioning in signaling pathways.

ACKNOWLEDGMENT

We thank the Laboratory of Chemical Physics at the National Institutes of Health and Dr. Frank Delaglio for making available NMRPipe, which were useful in analyzing our NMR data. We thank Ahmed Ahmed, Adrienne Loh, and Dawit Gizachew for helpful discussions.

REFERENCES

1. Barbacid, M. (1987) *ras* Genes, *Annu. Rev. Biochem. 56*, 779−827.
2. Bourne, H. R., Sanders, D. A., and McCormick, F. (1991) The GTPase superfamily: Conserved Structure and Molecular Mechanism, *Nature 349*, 117−127.
3. Hart, M., Eva, A., Evans, T., Aaronson, S., and Cerione, R. (1991) Catalysis of Guanine Nucleotide Exchange on the Cdc42Hs Protein by the *dbl* Oncogene Product, *Nature 354*, 311−314.
4. Horii, Y., Beeler, J. F., Sakaguchi, K., Tachibana, M., and Miki, T. (1994) A novel oncogene, ost, encodes a guanine nucleotide

exchange factor that potentially links Rho and Rac signaling pathways, *EMBO J. 13*, 4776−4786.

5. Leonard, D., Hart, M. J., Platko, J. V., Eva, A., Henzel, W., Evans, T., and Cerione, R. A. (1992) The identification and characterization of a GDP-dissociation inhibitor (GDI) for the CDC42Hs protein, *J. Biol. Chem. 267*, 22860−22868.
6. Farr, C. J., Saiki, R. K., Erlich, H. A., McCormick, F., and Marshall, C. J. (1988) Analysis of RAS gene mutations in acute myeloid leukemia by polymerase chain reaction and oligonucleotide probes, *Proc. Natl. Acad. Sci. U.S.A. 85*, 1629−1633.
7. Kiaris, H., Ergazaki, M., and Spandidos, D. A. (1995) Instability at the H-ras minisatellite is associated with the spontaneous abortion of the embryo, *Biochem. Biophys. Res. Commun. 214*, 788−792.
8. Shinohara, N., and Koyanagi, T. (2002) Ras signal transduction in carcinogenesis and progression of bladder cancer: Molecular target for treatment? *Urol. Res. 30*, 273−281.
9. Feltham, J. L., Dotsch, V., Raza, S., Manor, D., Cerione, R. A., Sutcliffe, M. J., Wagner, G., and Oswald, R. E. (1997) Definition of the switch surface in the solution structure of Cdc42Hs, *Biochemistry 36*, 8755−8766.
10. Pai, E. F., Kabsch, W., Krengel, U., Holmes, K. C., John, J., and Wittinghofer, A. (1989) Structure of the guanine nucleotide binding domain of the Ha-Ras oncogene product p21 in the triphosphate conformation, *Nature 341*, 209−214.
11. Pai, E. F., Krengel, U., Petsko, G. A., Goody, R. S., Kabsch, W., and Wittinghofer, A. (1990) Refined crystal structure of the triphosphate conformation of h-ras p21 at 1.35 Å resolution: Implication for the mechanism of GTP hydrolysis, *EMBO J. 9*, 2351−2359.
12. Hirshberg, M., Stockley, R. W., Dodson, G., and Webb, M. R. (1997) The crystal structure of human rac1, a member of the rho-family complexed with a GTP analogue, *Nat. Struct. Biol. 4*, 147−152.
13. deVos, A. M., Tong, L., Milburn, M., Matias, P., Jancarik, J., Miura, K., Noguchi, S., Nishimura, S., Ohtsuka, E., and Kim, S.-H. (1988) Three dimensional structure of an oncogene protein: Catalytic domain of human c-H-*Ras* p21, *Science 239*, 883−893.
14. Schlichting, I., John, J., Frech, M., Chardin, P., Wittinghofer, A., Zimmermann, H., and Roesch, P. (1990) Proton NMR Studies of Transforming and Nontransforming H-ras p21 Mutants, *Biochemistry 29*, 504−511.
15. Lin, R., Bagrodia, S., Cerione, R., and Manor, D. (1997) A novel Cdc42Hs mutant induces cellular transformation, *Curr. Biol. 7*, 794−797.
16. John, J., Frech, M., and Wittinghofer, A. (1988) Biochemical properties of Ha-ras encoded p21 mutants and mechanism of the autophosphorylation reaction, *J. Biol. Chem. 263*, 11792−11799.
17. Adams, P. D., Loh, A. P., and Oswald, R. E. (2004) Backbone dynamics of an oncogenic mutant of Cdc42Hs shows increased flexibility at the nucleotide-binding site, *Biochemistry 43*, 9968−9977.
18. Loh, A., Guo, W., Nicholson, L., and Oswald, R. E. (1999) Backbone dynamics of inactive, active, and effector-bound Cdc42Hs from measurements of ^{15}N relaxation parameters at multiple field strengths, *Biochemistry 38*, 12547−12557.
19. Guo, W., Sutcliffe, M. J., Cerione, R. A., and Oswald, R. E. (1998) Identification of the binding surface on Cdc42Hs for p21-activated kinase, *Biochemistry 37*, 14030−14037.
20. States, D., Haberkorn, R., and Ruben, D. (1982) A two-dimensional nuclear Overhauser experiment with pure absorption phase in four quadrants, *J. Magn. Reson. 48*, 282−292.
21. Delaglio, F., Grzeseik, S., Vuister, G. W., Zhu, G., Pfeifer, J., and Bax, A. (1995) NMRPipe: A multidimensional spectral processing system based on UNIX pipes, *J. Biomol. NMR 6*, 277−293.
22. Bartels, C., Xia, T.-H., Billeter, M., Guntert, T., and Wuthrich, K. (1995) The program XEASY for computer-supported NMR spectral analysis of biological macromolecules, *J. Biomol. NMR 5*, 1−10.
23. Otting, G., and Rückert, M. (2000) Alignment of biological macromolecules in novel nonionic liquid crystalline media for NMR experiments, *J. Am. Chem. Soc. 122*, 7793−7797.
24. Wishart, D. S., Sykes, B. D., and Richards, R. M. (1991) Relationship between nuclear magnetic resonance chemical shift and protein secondary structure, *J. Mol. Biol. 222*, 311−333.
25. Wishart, D. S., Sykes, B. D., and Richards, F. M. (1992) The chemical shift index: A fast and simple method for the assignment of protein secondary structure through NMR spectroscopy, *Biochemistry 31*, 1647−1651.
26. Schwieters, C. D., Kuszewski, J. J., Tjandra, N., and Clore, G. M. (2003) The Xplor-NIH NMR molecular structure determination package, *J. Magn. Reson. 160*, 65−73.
27. Guex, N., and Peitsch, M. C. (1997) SWISS-MODEL and the Swiss-PdbViewer: An environment for comparative protein modeling, *Electrophoresis 18*, 2714−2723.
28. DeLano, W. L. (2002) The PyMol molecular graphics system, http://www.pymol.org.
29. Laskowski, R. A., Rullmannn, J. A., MacArthur, M. W., Kaptein, R., and Thornton, J. M. (1996) AQUA and PROCHECK-NMR: Programs for checking the quality of protein structures solved by NMR, *J. Biomol. NMR 8*, 477−486.
30. Kelley, L. A., and Sutcliffe, M. J. (1997) OLDERADO: On-line database of ensemble representatives and domains, *Protein Sci. 6*, 2628−2630.
31. Wittinghofer, A., and Pai, E. (1991) The Structure of Ras protein: A Model for a Universal Molecular Switch, *Trends Biomed. Sci. 16*, 382−387.
32. Redfield, A. G., and Papastavros, M. Z. (1990) NMR Study of the Phosphoryl Binding Loop in Purine Nucleotide Proteins: Evidence for Strong Hydrogen Bonding in Human N-ras p21, *Biochemistry 29*, 3509−3514.
33. Wuthrich, K. (1986) *NMR of Proteins and Nucleic Acids*, John Wiley and Sons, New York.
34. Reinstein, J., Schlichting, I., Frech, M., Goody, R., and Wittinghofer, A. (1991) p21 with a Phenylalanine 28 to Leucine Mutation Reacts Normally with the GTPase Activating Protein GAP but Nevertheless Has Transforming Properties, *J. Biol. Chem. 266*, 17700−17706.
35. Ramirez de Molina, A., Rodriguez-Gonzalez, A., and Lacal, J. C. (2004) From Ras signalling to ChoK inhibitors: A further advance in anticancer drug design, *Cancer Lett. 206*, 137−148.
36. Bos, J. L., Toksoz, D., Marshall, C. J., Verlaan-de Vries, M., Veeneman, G. H., van der Eb, A. J., van Boom, J. H., Janssen, J. W., and Steenvoorden, A. C. (1985) Amino-acid substitutions at codon 13 of the N-ras oncogene in human acute myeloid leukaemia, *Nature 315*, 726−730.
37. Hart, M. J., Eva, A., Zangrilli, D., Aaronson, S. A., Evans, T., Cerione, R. A., and Zheng, Y. (1994) Cellular transformation and guanine nucleotide exchange activity are catalyzed by a common domain on the dbl oncogene product, *J. Biol. Chem. 269*, 62−65.

BI051686G